Visualization of Tight-Binding Calculations—The Electronic Structure and Electron Localization of the Si(100) Surface

Thomas F. Fässler,* Ulrich Häussermann and Reinhard Nesper

Dedicated to Professor Gerhard Thiele on the occasion of his 60th birthday

Abstract: The advantage of computer graphics in the visualization of tight-binding calculations is highlighted in a model study of the reconstruction of the Si(100) surface. Three different surface models—the unreconstructed surface Si(100)-(1×1), and symmetric and asymmetric pairing of surface atoms Si(100)-(2×1)—are investigated on the basis of density of states (DOS), local (projected) density of states (LDOS) and crystal orbital-overlap population (COOP) analysis. For the visualization of the real-space properties of tight-binding calculations, two- and three-dimensional images of the total (TED) and partial electron densities (PED) are shown. The PED calculated near the Fermi level are compared to densities of HOMOs and LUMOs in molecular systems and used to analyse constant current mode STM images, obtained by applying bias voltages of different sign. They show excellent agreement with STM experiments. The electron-localization function (ELF) has been shown to describe chemical bonds in molecules and solids surprisingly well. Here, the ELF is calculated for surfaces. In order to visualize the shape of the "dangling" surface bonds and bonds connecting surface atoms, two- and three-dimensional representations of the ELF are discussed. Using the reconstruction of the Si(100) surface as an example, we show that combining methods for extracting information from quantum mechanical calculations, such as PED, TED and ELF, leads to a more comprehensive description of the electronic surface structure. With the help of computer graphics, chemical concepts routinely used for describing local properties of molecules can be transferred very effectively to extended systems.

Keywords
chemical bonding · electron localization · scanning tunnelling microscopy · surface structures · tight-binding calculations

Introduction

1. General remarks: Surface chemistry, despite its industrial importance in areas such as heterogeneous catalysis and thin-film formation, is still a very descriptive discipline. Although a large number of experimental methods for studying surface structures and reactivities now exist, for many surfaces no consensus has yet been reached as to the arrangement of surface atoms and adsorbates, and, hence, the related area of electronic structure has also not been adequately described. What controls the shape of surfaces? Why do many surfaces reconstruct and what determines the resulting geometry? Why are very specific adsorption patterns of small molecules or atoms on surfaces frequently observed? Most of these phenomena are just beginning to be understood.

Remarkable developments in the field of surface analysis, such as scanning tunnelling (STM) and atomic force microscopy (AFM), have turned out to be very powerful tools for the investigation of the local and extended structures of surfaces. Results of STM experiments reflect the electronic structure and geometry of surfaces and may thus help in the development of chemical concepts to explain the reactivity and stability of surfaces. Despite its great potential, STM often yields pictures and surface models that are not uniquely interpretable, and, in many cases, the distribution and localization of the electrons on a surface cannot be ascertained.[1] Experimental chemists need additional chemical concepts to understand the reactivity of a specific surface and to derive possible heterogeneous reactions.[2]

Many rules, models and concepts, for example, the Lewis formulae,[3] orbital hybridization,[4] VSEPR (valence-shell electron-pair repulsion rules)[5] and Wade rules,[6] are available to the chemist to help explain and predict the shape and reactivity of molecules. On a more sophisticated level we can determine the electronic structure of a molecule, to a certain degree of approximation, by solving the Schrödinger equation. Deriving the energy, symmetry and shape of molecular orbitals, we gain a considerable amount of information on the reactivity of the system. Thus many reactions can be understood by using localized orbitals[7a] and/or the frontier orbital approach.[7b] But how far can we develop similar ideas for extended systems?

To gain insight into the electronic structure of an extended surface, we can, in principle, apply the same principles as for molecules, taking advantage of the periodicity of the surface in two dimensions. However, approximation of the third dimension by using a multilayer slab model, which resembles the bulk, leads to an increased orbital basis set. By forming Bloch func-

[*] Dr. T. F. Fässler, Dipl.-Chem. U. Häussermann, Prof. R. Nesper
Laboratorium für Anorganische Chemie der
Eidgenössischen Technischen Hochschule
Universitätstrasse 6, CH-8092 Zürich (Switzerland)
Telefax: Int. code + (1)632-1149
e-mail: faessler@inorg.chem.ethz.ch

  0947-6539/95/0109-0625 $ 10.00+.25/0

tions within the first Brillouin zone and calculating energy levels for a specific number of grid points (k points) in reciprocal space, we can analyse the band structure. As soon as the number of energy levels increases, band-structure diagrams become highly complex, and thus often difficult to interpret, even when represented only along k points of high symmetry, as is normally the case.[8] For specific points in reciprocal space it is possible to represent the wave function, though this becomes very convoluted for problems with a large number of atoms and orbitals, respectively.

Quantum-mechanical calculations can also be interpreted by looking at the energy-level distribution (averaged over the weighted k points in reciprocal space). By plotting the density of states (DOS = number of energy levels between E and $E + \Delta E$) versus the energy and projecting the DOS on orbitals or orbital groups of the basis set (LDOS = local or projected DOS), we obtain information how the electrons are distributed among orbitals or atoms. Finally, to find bonds in extended systems we can apply the extended concept of the Mulliken overlap populations to the totally delocalized crystal orbitals (CO), the so-called COOP method (COOP = crystal orbital-overlap population).[9] All these methods, however, do not provide information about the *spatial electron distributions*, the *shapes of frontier orbitals (bands)* in real space, the *localization of electrons*—in two-centre/two-electron bonds, three-centre/two-electron bonds or lone pairs—or their delocalization over the entire system.[10]

Here we show how electronic structure and chemical bonding for extended two-dimensional systems can be represented in direct space by the use of appropiate projection methods and two- and three-dimensional computer graphics. This is achieved by transforming the eigenfunctions of all occupied energy levels (total DOS or TDOS) or of only a selection of levels within an energy window (partial DOS or PDOS) into the total electron density (TED) or a partial electron density (PED), respectively. By choosing the energy window just below or above the Fermi level for the given electron count of a chemical system, we obtain images of the partial electron density derived from crystal orbitals corresponding to virtual electron densities of HOMO and LUMO states in molecular systems, respectively. In order to visualize chemical bonds or other regions of localized electrons (e.g., lone pairs), we use the electron localization function (ELF) based on the method of Becke and Edgecombe[11] for surfaces. The ELF has proven to be a very powerful method to describe bonds as well as lone pairs in molecules[12] and was recently applied to extended three-dimensional systems, too.[13] It is even possible to generate a new classification of chemical bonding.[13b,c]

2. The Si(100) surface: Although Si(100) is one of the most studied surfaces, there is a long debate in literature about its geometrical and electronic structure.[14] Generation of an unreconstructed (100) surface from a solid with diamond structure leads to exclusively two-coordinate surface atoms (Fig. 1a), instead of four-coordinate as in the bulk. The resulting two unshared valencies at each surface atom are the so-called "dangling bonds".

From a large body of experimental data, it is known that this surface is unstable and undergoes a 2×1 reconstruction.[15-18] There are numerous models describing the reconstruction, two of which are most likely to be accurate. In both models (Fig. 1b·c), two surface atoms form a dimeric unit by approaching each other and reducing the number of unshared valencies for each surface atom from two to one. However, no consensus has yet been found as to whether the dimer formation is symmetric[14, 17, 18] (Fig. 1b) or asymmetric[19] (buckled, Fig. 1c). The results from a number of experimental[20-22] and theoretical investigations[23-27] can be used to support either of these models. Various calculations slightly favour the asymmetric over the symmetric dimer model.[24, 26] However, models that take spin arrangements into consideration point to the latter as being more stable.[23a]

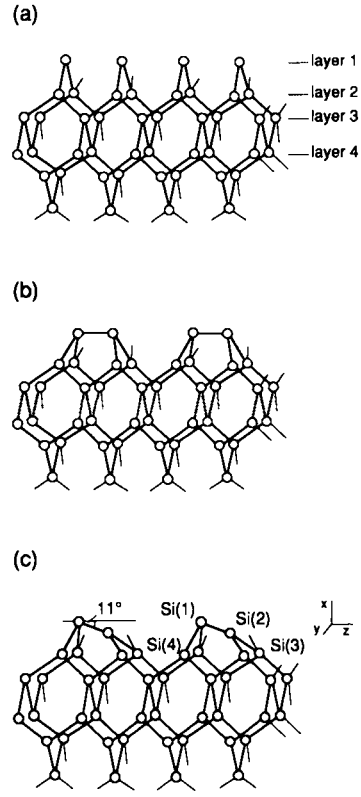

Fig. 1. Atomic arrangement of the diamond structure terminated at a 100 plane. a) (1×1) Unreconstructed, terminated bulk structure. b) (2×1) Symmetric reconstruction. c) (2×1) Asymmetric (buckled) reconstruction. In each case the six topmost layers are shown.

STM experiments on clean Si(100) surfaces confirm that both symmetric and asymmetric dimers are present.[20-22] The degree of asymmetry may change in different domains of the silicon surface detected during the STM experiment. A higher degree of asymmetric dimer formation is found at low temperatures[20a] or in areas of the surface adjacent to regions where surface atoms are missing (surface defects).[20b] The degree of asymmetry observed in a surface region is also found to depend on the sign of the bias voltage used during the experiment.[20c, 22] Figure 2 displays a reproduction of the STM

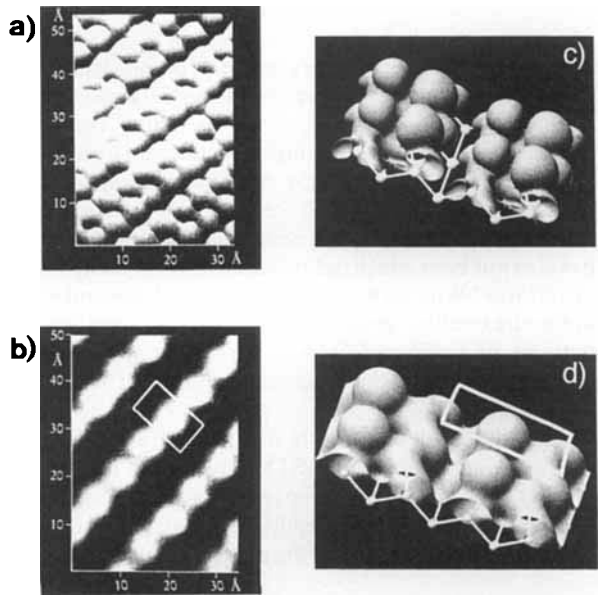

Fig. 2. a) STM image of Si(100) obtained with positive bias voltage. Symmetric dimers are visible. b) STM image of Si(100) obtained with negative bias voltage. Only one surface atom of the dimer is visible (a and b reproduced from ref. [22]). c) Three-dimensional image of an isosurface of the PED of the buckled surface structure. The PED is calculated using the band levels above the Fermi level (E_f to $E_f + 3$ eV). d) As in c), using band levels below the Fermi level (E_f to $E_f - 3$ eV). Four unit cells are shown; for isovalues see Figure 5.

0947-6539/95/0109-0626 $ 10.00+.25/0 Chem. Eur. J. 1995, 1, No. 9

images of the same domain of a clean Si(100) surface for a positive (Fig. 2a) and negative (Fig. 2b) bias voltage.[22a] The fact that the STM images change with the sign of the bias voltage indicates that the electronic contribution to the STM images is dominant in this particular case.[22b]

According to the approach of Tersoff and Hamann for interpreting STM images,[28] the STM tunnelling current between a surface sample and an STM tip is a function of the electron density of the surface states (i.e., contributions from the atoms of the surface layers). This is valid for surface states close to the Fermi level. Depending on the sign of the bias voltage used for the STM experiment, electrons either tunnel from the STM tip to empty surface states (positive bias; Scheme 1: electron transfer from b) to a) indicated by fields with criss-cross shading and a solid arrow; empty-state image) or from filled surface states to the STM tip (negative bias; Scheme 1: electron transfer from a) to b) indicated by striped fields and broken arrow; filled-state image). For larger distances between STM tip and surface (>4 Å), the interaction of the states of the tip with those of the surface can be neglected,[29, 30b] and the tunnelling current, and thus the brightness of the STM image, becomes proportional to the density of states at the surface (LDOS).[28]

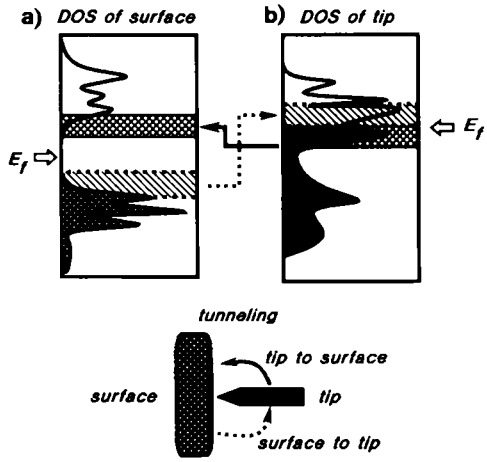

Scheme 1.

Generally the STM images of the Si(100)-(2 × 1) surface are interpreted as follows: filled-state images, consisting of rows of oval areas (Fig. 2b) originate from tunnelling from π-type bonding orbitals of pairs of silicon atoms of symmetric dimers.[20c] The occasional presence of zig-zag structures (instead of rows) are interpreted as tunnelling from states arising from rows of buckled dimers. Here, the direction of buckling alternates from dimer to dimer along the row. Empty-state images always show rows of predominantly symmetric dimers (Fig. 2a). The two silicon atoms forming the dimer are well separated by a minimum. In some cases a small degree of asymmetry can be observed.[21b] The π* antibonding states have been proposed to take part in this tunnelling process.[20c]

It is remarkable that buckling of the dimers appears only when the filled states are used for imaging, that is, when electrons tunnel from the highest occupied electronic levels of the solid to the empty levels of the metal tip.

An approach to modelling these Si(100)-(2 × 1) STM images[30a] is the calculation of the self-consistent charge density of filled and empty surface states.[27] Here, however, specific points in reciprocal space are chosen to fit the observed images.[30a] Recent publications of M.-H. Whangbo et al.[30b] show that, for several layered transition-metal chalcogenides and transition-metal halides, the results of local (partial) electron-density calculations (averaged over the first Brillouin zone) on the basis of the extended Hückel tight-binding method (EHTB)[31] are in good agreement with the observed STM images. Our calculations used here are also based on the EHTB approach. A 16-layer slab model was used to calculate the surface properties of bulk silicon (see Computational Details).

In order to show the advantage of real-space representations of electron distributions on surfaces with three-dimensional resolution in direct space, we have calculated images of TED, PED and ELF for the extensively studied Si(100) surface. These images are compared with results obtained by "classical" interpretation of band-structure calculations by calculating the DOS, LDOS and COOP. Finally we discuss how these electron-distribution images correspond to those obtained experimentally by STM techniques.

Results and Discussion

1. Electronic structure of the Si(100) surface studied by density of states methods: To study the influence of surface geometry on the electronic structure we performed several tight-binding calculations. They were carried out for the unreconstructed surface and for two idealized models of the reconstructed surface (symmetric and asymmetric dimer formation). To avoid problems with the coordination number[32] for the three surfaces under consideration, we kept all bond lengths the same as within the bulk (2.35 Å).

Figure 3 shows DOS diagrams of bulk silicon (Fig. 3a), of the unreconstructed Si(100)-(1 × 1) (Fig. 3b), and of the symmetrically (Fig. 3c) and asymmetrically reconstructed surface Si(100)-(2 × 1) (Fig. 3d). The projection on the orbitals of the surface layer (surface states) is shown in black. Note that the surface states are pushed up in energy compared to the bulk

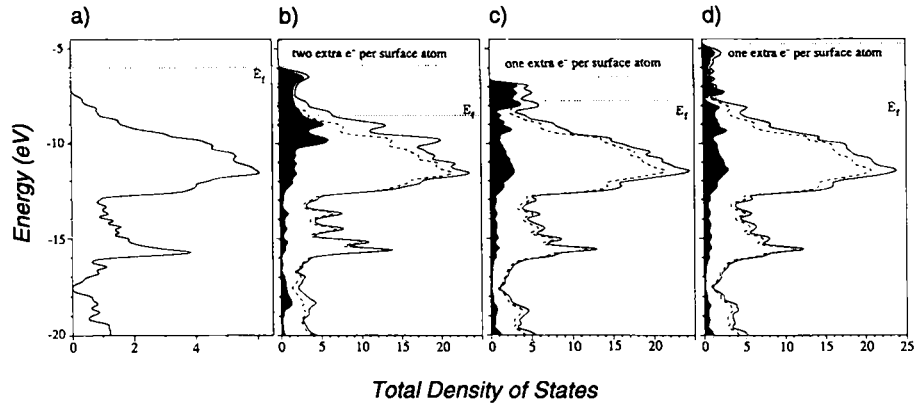

Fig. 3. Total density of states plots (solid line) of a) bulk silicon, b) the unreconstructed Si(100)-(1 × 1) surface structure, c) the reconstructed Si(100)-(2 × 1) structure with symmetric dimers, and d) the reconstructed Si(100)-(2 × 1) surface structure with asymmetric (buckled) dimers. Black areas and dashed lines in b), c) and d) show the contributions of the surface and bulk atoms, respectively. Band occupancy according to the electron count of elemental silicon is indicated by a dotted line labelled E_f. The upper dotted lines correspond to higher band occupancies (see text).

states. The surface atoms have fewer nearest neighbours, and there is thus less orbital interaction. As a result the nonbonding states are at the top of the valence band. The levels obtained by filling the band to be consistent with the electron count of silicon (E_f) and further up to the top of the valence band are indicated as horizontal dotted lines. In the case of the unreconstructed (1×1) surface (Fig. 3b) the top of the filled bands corresponding to the electron count of silicon (E_f, dashed line in Fig. 3b) cuts a region of high surface-state density. Whenever a distortion is possible to reduce this density, it will occur. This is the case, for example, in Peierls-type or Jahn–Teller distortions.[2c] The surface structure in Figure 1a is expected to show metallic behaviour, in contrast to experiment.[19a] With the addition of two further electrons per surface atom, the entire valence band is filled (upper dashed line in Fig. 3b). This corresponds to the formation of two lone pairs at each surface atom, which are then isoelectronic to sulfur atoms. For the symmetrically distorted (2×1) surface, the surface atoms are now triply bound, and E_f still cuts a region with a high density of states. The valence band is filled when one extra electron per surface atom is added (upper dashed line in Fig. 3c); the residual "dangling" bond is coverted into a lone pair. Thus, tilting the dimer unit by an angle of 11°[33] (Fig. 1c, Fig. 3d), we find, for the electron count of silicon (E_f, dotted line), a minimum in the total DOS and a small gap in the projected DOS of the surface states. As for the symmetric reconstruction model, the valence band becomes completely filled by addition of one extra electron per surface atom (upper dashed line). The surface atoms remain triply bound and are then isoelectronic to phosphorus atoms.

More detailed information is expressed by the DOS projections on the surface atoms. Figure 4 shows the s, $p_y + p_z$ (the *yz* plane is parallel to the surface) and p_x contributions of the surface orbitals (see Fig. 1 for axes) to the total DOS near the Fermi level (± 4 eV). The contributions of the surface states are shown as filled (s orbitals), dotted ($p_y + p_z$ orbitals) and dashed (p_x orbitals) lines. The total density of the surface states (cf. black area in Fig. 3b–d) is represented by the solid line. For the unreconstructed surface (Fig. 4a) we see that above E_f mainly p_y and p_z orbitals contribute to the LDOS, whereas below E_f all the p orbitals and the s orbital contribute. In the case of the symmetrically distorted surface model (Fig. 4b), the p_x and s states are pushed up in energy, and the p_y and p_z contributions down. Clearly, this arises from the orbital interactions within the *yz* plane forming the surface dimer bonds.

Finally, formation of the *asymmetric* dimer leads to two unequal surface atoms (Fig. 4c, d). Our calculations show, that the LDOS within the upper and lower energy windows (E_f to $E_f + 3$ eV and E_f to $E_f - 3$ eV, respectively) are almost purely due to p_x orbital contributions of the surface atoms Si(2) and Si(1) (Fig. 1c), respectively. The p_x states of the outer atom, Si(1), are pushed below E_f (Fig. 4c), and p_x states arising from the inner atom, Si(2), are pushed above E_f (Fig. 4d). This leads to a charge transfer from atom Si(2) to Si(1) (Mulliken charges are $q(\mathrm{Si(1)}) = 4.92$, $q(\mathrm{Si(2)}) = 3.50$). From a qualitative point of view, this results in the formation of a lone pair at Si(1) and an empty orbital with mainly p_x contribution at Si(2). The shifting of energy levels can be explained in terms of the following qualitative molecular model: flattening of the coordination at Si(2) and, hence, the reduction of s contribution to the unoccupied orbital leads to a shift of the state to higher energy, while the decrease of the bond angles at Si(1) gives rise to a bigger s contribution to the lone pair, a corresponding lowering of the energy and complete occupation of this state (Fig. 4f, g). Use of a more sophisticated asymmetric distortion, for example, relaxation of atoms down to the fourth surface layer,[24d] leaves the resulting DOS and related projections almost unchanged.

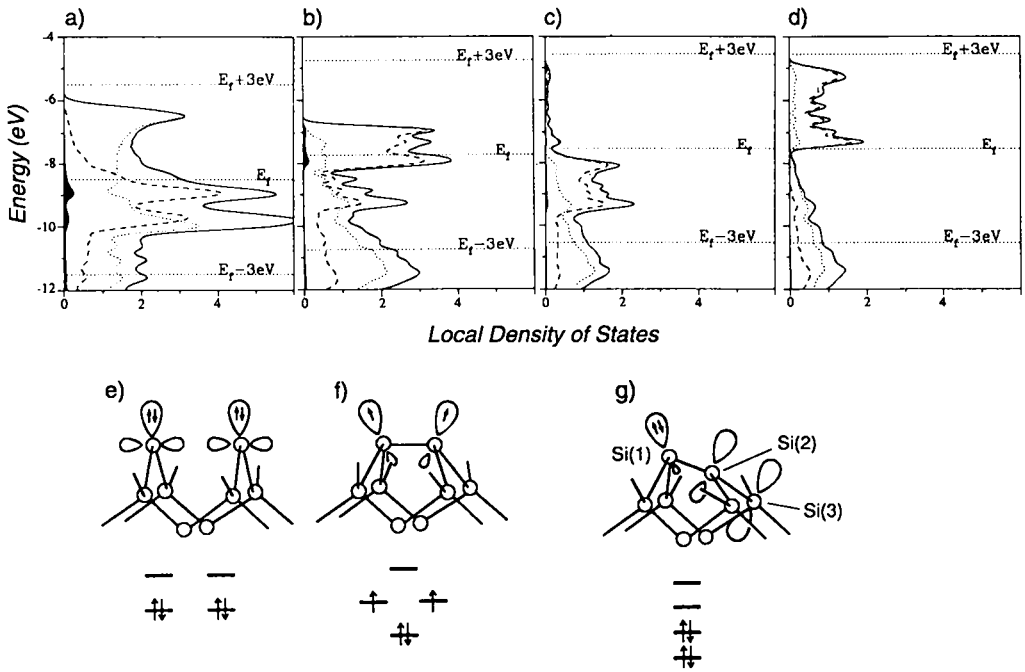

Fig. 4. Local density of states and orbital contributions near the Fermi level for the topmost surface layer, calculated for the three surface structures shown in Fig. 1. The projected orbital contributions are represented as follows: total density of surface states as solid lines, p_x as dashed lines, $p_y + p_z$ as dotted lines, and s as black areas. a) Si(100)-(1×1), unreconstructed surface, b) Si(100)-(2×1) with symmetric dimers; c) and d) show the contribution of the two different surface atoms Si(1) and Si(2) of Si(100)-(2×1) with asymmetric (buckled) dimers, respectively; for labelling see Figure 1c. The horizontal dotted lines indicate the energy windows used for the PED diagrams in Figures 2, 5 and 6 (E_f to $E_f \pm 3$ eV). e)–g) show the shapes of hybrid orbitals deduced from band structure and PED calculations (see text).

DOS and LDOS vs. energy diagrams are useful for the discussion of band occupancy, of band gaps and therefore of stability, but they do not tell us anything about the actual appearance of the related frontier crystal orbitals and the geometrical distribution of the electron density, for example, whether the sp hybrids with p_x contributions point away from the surface or toward the bulk. The representation of the wave function at points of specific symmetry in reciprocal space is possible (e.g., at Γ). At general points, however, the wave function has an imaginary term and can not be shown in direct space, right away. In contrast, the total electron density is an observable quantity and has a representation in direct space.

0947-6539/95/0109-0628 $ 10.00+.25/0 Chem. Eur. J. 1995, 1, No. 9

2. Electronic structure of the Si(100) surface in terms of real-space representations: Figures 5a–c show contour plots of the TED for the three surface structures under discussion, for the electron count of silicon. The densities on a plane perpendicular to the surface and parallel to the silicon–silicon dimer bond are displayed. In Figures 6a–c selected isovalues (cf. Figs. 5a–c) of the total electron density of the topmost surface layer are shown as three-dimensional images. From Figure 5a and 6a we can see that the density arising from the two "dangling bonds" at each surface atom of the unreconstructed surface form an almost circular region directly above each surface atom, but merge continously into the density of the intact bonds, which are directed toward the bulk. By formation of symmetric dimers the latter density diminishes, and the electron density between the two surface atoms increases (Fig. 5b, 6b). Tilting the dimer bond leads to a loss of electron density at the less exposed Si(2) atom, and an increase at the outer surface atom Si(1) (Figs. 5c, 6c). The appearance of a "hole" in the electron density at the innner atom Si(2) in Figure 6c is due to the fact that only valence electrons are included in the calculations and that the p_x orbital of Si(2), which extends in the x direction, is not occupied. For the former reason the electron density vanishes at the silicon cores in Figure 5, too.

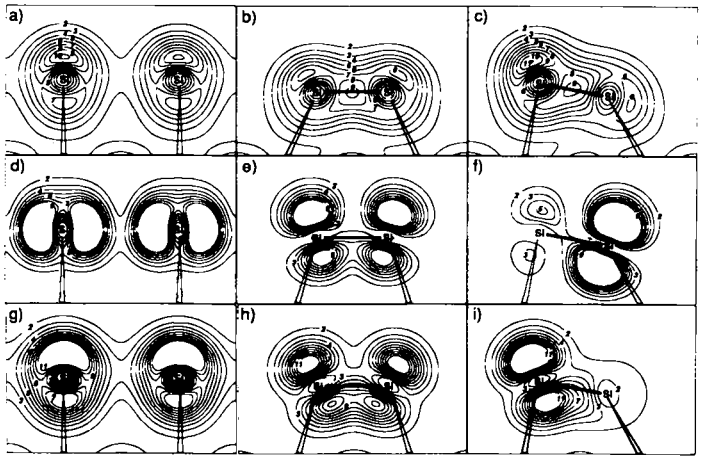

Fig. 5. Contour plots of electron densities of a surface section of the unreconstructed (a, d, g), symmetric (b, e, h) and asymmetric (c, f, i) surface structures. The plane perpendicular to the surface passing through the two surface atoms Si(1) and Si(2) is shown (cf. Fig. 1). a), b) and c): contour plots of the TED. d), e) and f): PED using band levels above the Fermi level (E_f to $E_f + 3$ eV). g), h) and i) PED using band levels below the Fermi level (E_f to $E_f - 3$ eV). The contour values are given in 5×10^{-3} a.u. for a)–c), 2×10^{-3} a.u. for d)–f), and 3×10^{-3} a.u. for g)–i) (a.u. = atomic units).

In order to visualize the degree of orbital mixing at the surface, we calculated the PED within energy windows of 3 eV below and above E_f (E_f to $E_f - 3$ eV and E_f to $E_f + 3$ eV, respectively). The computed contour plots and isosurfaces of PED now display densities with the characteristics of highest occupied (HOCO, Figs. 5g–i) and lowest unoccupied (LUCO, Figs. 5d–f) crystal orbitals averaged over the first Brillouin zone (see Computational Details), corresponding to virtual HOMO and LUMO densities in molecules.[34] Although the PED images are generated from all levels within the energy window, the main contributions in the chosen part close to the Fermi level are dominated by surface states (filled areas in Fig. 3) and therefore correspond to LDOS at the Fermi level. Contributions of bulk atoms to the PED would anyway not appear in the selected spatial region.

From Figures 5d and 6d it is obvious that the density of the LUCO of the undistorted surface is composed of p_z orbitals only, whereas, below the Fermi level, s and p mixing leads to hybrids (HOCO) perpendicular to the surface, pointing toward the vacuum (Figs. 5g and 6g). For the symmetric dimer, LUCO (Fig. 5e and 6e) and HOCO (Fig. 5h and 6h) densities are tilted away from the surface normal, retaining the mirror plane perpendicular to the dimer bond. The orbital tilt is the result of partial p_x–p_z orbital mixing. The tilt angles between the surface hybrids and the surface dimer bond are 120° for the HOCO and 105° for the LUCO. The situation in the case of the asymmetrically distorted surface is different. The contribution of Si(2) dominates in the LUCO (Figs. 5f, 6f), and that of Si(1) in the HOCO (Fig. 5i, 6i). However, as it can be seen from Figure 5f, there is some LUCO density above the outer surface atom Si(1), whereas no substantial HOCO density is found above Si(2) (Fig. 5i). The tilt angles with respect to the (100) plane are 75 and 70° for the LUCO above Si(1) and Si(2), respectively, and 110° for the HOCO above Si(1) (calculated using the maxima of the PEDs above the surface atoms in Figs. 5f and 5i). These PED images reflect the shape of hybrid orbitals that could be derived for molecules (Figs. 3e–g).

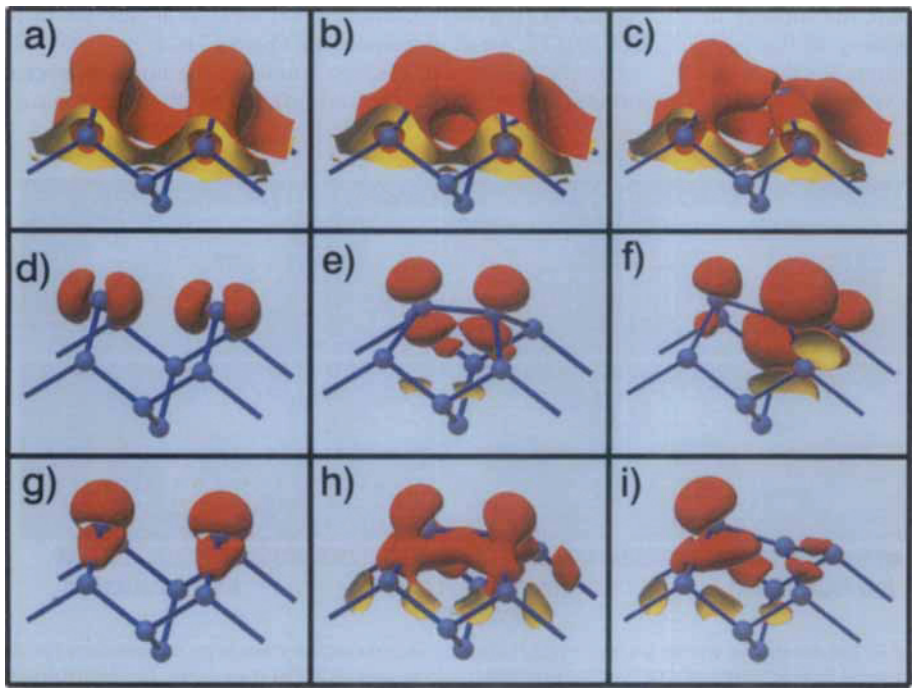

Fig. 6. Isodensity surfaces of a section of the unreconstructed (a, d, g), symmetric (b, e, h) and asymmetric (c, f, i) surface structures. a), b) and c): TED. d), e) and f): PED using band levels above the Fermi level (E_f to $E_f + 3$ eV). g), h) and i): PED using band levels below the Fermi level (E_f to $E_f - 3$ eV). For further explanations of the structures and the units of the isosurfaces see caption to Figure 5.

  0947-6539/95/0109-0629 $ 10.00+.25/0

3. Interpretation of the STM images: Since the PED calculations detect the *occupied surface* states locally at a symmetric surface dimer, they are expected to yield a bean-shaped spot with a local minimum between the two silicon atoms (Fig. 5h), such as that found in the STM experiments.[20c, 40] In the case of asymmetric dimers only states located at Si(1) atoms can contribute to the PED and, thus, to the white areas of the STM images. Therefore, in the STM image of the Si(100) surface, only one surface atom per dimer will be observed for asymmetric dimers. With the same orientation of the buckling along one row of dimers, we expect an image similar to Figure 2b. Alternate orientation of the buckling will lead to zig-zag structures. For large surface regions where only a line of single maxima along the directions of rows of surface dimers are detected,[22a, 22c] it is not clear whether these arise from buckled or symmetric dimers. However, if the white spots are due to symmetric dimers, they should have a more oval shape. Considering the *empty surface* states, all surface atoms show PED contributions with well-separated maxima above the surface. This is quite similar for symmetric (Fig. 5e) and asymmetric (Fig. 5f) surface dimers. The Si(100) surface appears in this case as an arrangement of symmetric dimer units in the STM image (Fig. 2a). To compare the STM images shown here[22a] with our calculations, the LUCO and HOCO densities for the asymmetric dimer formation have been calculated for four unit cells. Comparison of Figure 2a with 2c and Figure 2b with 2d reveals the remarkable agreement with the experimental STM images. The values of the isosurfaces are given in Figure 5f and 5i.

4. Electron localization on the Si(100) surface: The representations of the electron densities (TED and PED) give us some idea of how the electrons are distributed at the surface, but do not clearly show the characteristics of the chemical bonding. To detect the chemical bond between two atoms, the extended concept of Mulliken populations, the COOP vs. energy diagram,[9] can generally be used. The integral up to the Fermi level gives the total overlap population for a particular band, which scales like the bond order of this bond. To estimate the stability of different bonds we can compare the corresponding overlap populations. For bulk silicon the overlap population for the Si–Si bond is calculated to 0.839. Reconstruction with dimer formation results in a higher overlap population for the newly formed surface dimer bond (within the first layer) for both symmetric and asymmetric surface structures (Table 1). In the case of symmetric dimer formation, the surface–bulk bond is weakened (bond from the first to the second layer). For the asymmetric surface structure, however, the two different surface–bulk bonds (Si(1)–Si(4) and Si(2)–Si(3), cf. Fig. 1) are much stronger and the overlap populations are close to that calculated for bulk silicon.

To learn more about the spatial characteristics such as π bonding or the characteristic of bent bonds, we need more sophisticated methods. For example, the break down of the related COOP with the help of DOS and LDOS curves[2c] is not straightforward when strong orbital mixing (low symmetry) is involved and fails to yield information about the shape and orientation of nonbonding states like lone pairs.

Table 1. Overlap populations calculated for the bonds occurring in the two topmost layers of the reconstruction models shown in Figures 1b and c.

surface structure	Si(1)–Si(2)	Si(1)–Si(4)	Si(2)–Si(3)
symmetric dimer	0.943	0.481	0.481
asymmetric dimer	0.959	0.776	0.874

A usefull tool for deriving three-dimensional images of chemical bonding and also of lone-pair regions is the electron localization function (ELF), which leads to a detailed picture of electron distributions.[11] Typically σ bonds have localization regions with rotational symmetry along the line connecting atomic nuclei. For π bonds the region of localization is smaller along this line, but larger above and below. The region of high localization is thus shaped like a dumbbell, placed between the two atoms perpendicular to the plane of the molecule.[12]

Figures 7 and 8 show two- and three-dimensional representations of the ELF for the three surface structures (Figs. 1a–c). Figure 7, which represents the same planes as in Figure 5, contains two types of information: the density of points is a measure of the electron density, and the colour of each pixel codes the value of the ELF (see colour bar at the bottom of Figure 7: right (white), ELF = 1.0; middle, ELF = 0.5; left, ELF > 0.0). Lighter colours represent higher values of ELF and hence regions of preferred electron localization. Figures 7d–f show the ELF for an electron count corresponding to that of silicon. In Figures 7a–c the electron counts are such that the entire valence band is filled (see upper dashed line in Figs. 3b–d). This partial reduction is formally an addition of two further electrons per surface atom for the surface structure in Figure 1a, but only one further electron per surface atom for the surface structures in Figures 1b and 1c. Figure 7 can be read as a table with increasing electron number from bottom to top (d → a, e → b, f → c) and each column (a·d; b·e; c·f) representing one surface model. Figures 8a–f give three-dimensional views of isosurfaces with ELF = 0.75, which correspond to Figures 7a–f.

For the two chosen electron counts in the unreconstructed surface (Figures 7a, 7d, 8a and 8d), we see that electrons are

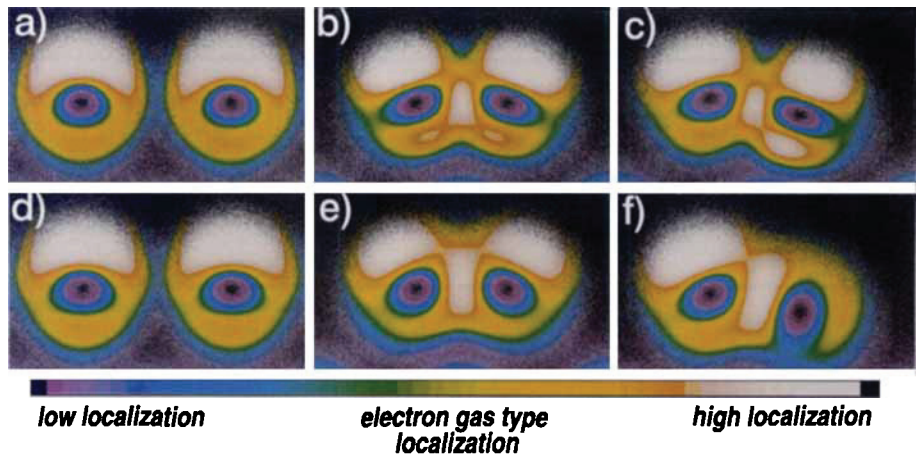

Fig. 7. Two-dimensional representation of the ELF. Planes through the surface atoms of the unreconstructed (a, d), symmetric (b, e) and asymmetric (c, f) surface structures (planes analoguous to Fig. 5) are shown. The electron density is given by the density of the pixels, and the colour of each pixel is a measure of ELF [12] ($0 < ELF \leq 1$). The lighter the colour the higher the ELF value. White regions represent areas of bonding electrons and lone pairs. The second row (d–f) corresponds to band occupancy appropriate for silicon (dotted horizontal line in Fig. 3b–d, labelled with E_f). The first row (a–c) corresponds to a partially reduced system, that is, a band filled with two (a) and one (b and c) additional electron per surface atom.

0947-6539/95/0109-0630 $ 10.00+.25/0 Chem. Eur. J. 1995, 1, No. 9

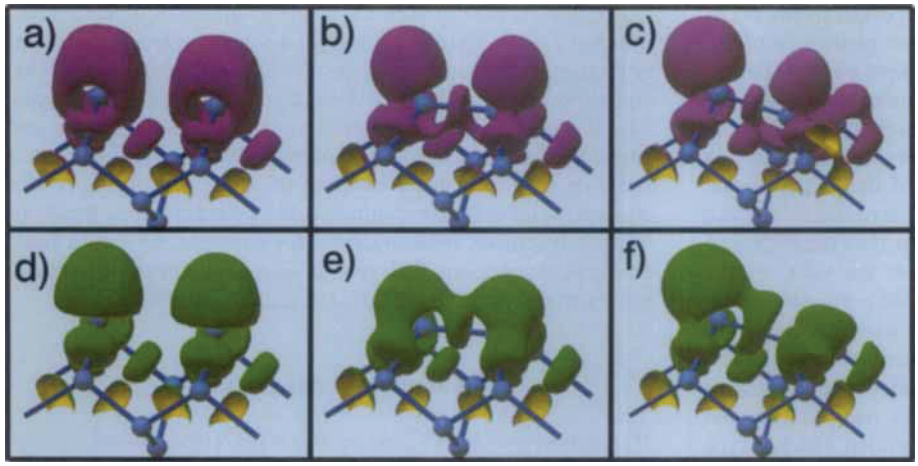

Fig. 8. Three-dimensional representation of isosurfaces of the electron localization function (ELF = 0.75). The sections of the two topmost layers of the two-dimensional unit cell for the three surface arrangements (cf. Fig. 1). The six representations correspond to the two-dimensional sections of Figures 7a–f.

localized (white regions) above the doubly coordinated surface atoms; this corresponds to two (Figs. 7a and 8a) and one lone pair at each surface atom (Fig. 7d and 8d), respectively. With the formation of a symmetric dimer bond, electrons are localized between the two surface atoms (Fig. 7e and 8e). Now, the white areas qualitatively resemble a two-centre/two-electron bond and two dangling bonds, holding one electron each. Partial reduction (Figs. 7b and 8b) leads to an increase in size of the lone-pair region. It is to be expected that, as the lone-pair states are gradually filled, the localization area along the Si–Si surface bond becomes smaller and vice versa.[35]

When the dimer is tilted and the asymmetric dimer formed, a shift of electron localization from Si(2) to Si(1) (Fig. 7f and 8f) is observed, which is correlated to the shift of the electron density. It should be noted that this is not generally the case.[12] The shape of the lone pair localized at the outer silicon atom of the buckled dimer (Fig. 8f) is very similar to the one found in the partially reduced system of the symmetric surface dimer (Fig. 8b). Both correspond to localization areas of one nonbonding electron pair. Consequently, partial reduction leads to the formation of the other lone pair at Si(2), leaving the shape of the first one nearly unaltered (Figs. 7c, 8c). In the cases of Figure 8e and 8f we find that the sections corresponding to Si(1)–Si(2) and Si(2)–Si(3) bonds have well developed extensions in x direction and perpendicular to the interatomic direction. Here, the lone-pair regions overlap with the localization regions of the Si–Si bonds. This is a typical π-bond characteristic, and it is most pronounced between Si(2) and Si(3) in the buckled dimer model (Fig. 8f).

5. The chemical bond: In order to understand the chemical bonding along the surface bonds, we can look at the local coordination spheres of the silicon atoms. Formation of the buckled dimer generates specific coordination types: distorted trigonal pyramidal for Si(1), almost trigonal planar for Si(2) and distorted trigonal bipyramidal with one missing axial position for Si(3) (Fig. 4g). Thus, at all silicon atoms of the first and second layers, which are exposed to the vacuum, sp hybrid orbitals can be formed, pointing away from the surface and with different amounts of s and p orbital contributions.

The local environments of the silicon atoms in the two topmost surface layers of this reconstruction model are also found in other silicon-containing materials. In $CaSi_2$[36] the anionic silicon substructure forms a structure that can be regarded as being isoelectronic to that of α-arsenic, containing atoms coordinated in a trigonal-pyramidal fashion, similar to Si(1). Formal electron transfer from calcium to silicon results in filled hybrid orbitals at the silicon atoms, which then become isoelectronic to phosphorus. An analogue to Si(2) is found in the trigonal-planar $SiSi_3$ unit in silicides, for example, in $Ca_{1.65}Li_{1.85}Si_7$.[37] An example of the coordination mode of Si(3) is found among the class of pentacoordinated silicon atoms. In $R_4Si{\leftarrow}NR'_3$ the silicon atom has a trigonal-bipyramidal coordination sphere.[38] An alternative description is of a central silicon atom with four covalent bonds forming a trigonal-pyramidal coordination sphere (similar to the one around Si(3)) and a donor–acceptor bond formed by the nitrogen lone pair and the empty hybrid orbital of the silicon atom.

For the (100) surface and an electron count corresponding to silicon, the hybrid orbital at Si(1) is filled (HOCO, Fig. 6i), and a lone pair is thus formed (Fig. 8f). The orbital localized at Si(2) (which has almost no s-orbital contribution) and that at Si(3) are unoccupied (Fig. 6f, the LUCO localized at Si(3) is cut in the middle). The shape of the localization regions along the Si(1)-Si(2)-Si(3) bonds shown in Figure 8f can now be understood in terms of the partial π character of this interaction, due to the conjugation of the lone pair at atom Si(1) and the two empty hybrid orbitals at Si(2) and Si(3), respectively (Fig. 4g).

These considerations allow us to transform the band-structure calculations into hybrid-orbital pictures (Figs. 4e–g). For the unreconstructed surface we have two empty and two filled orbitals (p_z and sp hybrids, respectively) per surface dimer unit localized at each surface atom (Figs. 6d, 6g and 4e). In the case of the symmetric dimer formation we find a lowering in energy of states forming the Si–Si surface bond (Fig. 6h) and two frontier orbitals (sp hybrids) with shapes shown in Figure 4f. Finally, buckling of the surface atoms results in the rehybridization shown in Figure 4g, as discussed above.

Summary and Conclusions

A model study of the reconstruction of the Si(100) surface has been undertaken to help visualize results of tight-binding calculations with the help of computer graphics. On the basis of the extended Hückel theory, three different types of surface structures are examined. In agreement with other calculations[22b, 26, 27] and experiment[19a] the surface becomes nonmetallic by formation of buckled (asymmetric) dimers. A minimum in the DOS and a gap in the surface DOS is found at E_f in the case of a dimer tilt angle of about 11°. Two- and three-dimensional pictures of the isosurfaces of the electron density and LDOS curves show that there is a charge transfer from the inner silicon surface atoms to the outer ones.

It has been shown that two- and three-dimensional representations of partial electron densities, for example, the electron density of the states within an energy window of 3 eV near the Fermi level, can be used to simulate STM images, both for positive and negative bias voltages. Clearly, the surface states

detected by STM techniques reflect the properties of the occupied states of the valence band and the unoccupied states of the conduction band. In agreement with experiment a higher degree of asymmetry of surface dimers is apparent in the filled-state image. This is well represented by the PED corresponding to the highest occupied crystal orbitals. Little or no asymmetry is found in the representations of the PED of the empty states, even though they were calculated from the asymmetric surface model. However, we would like to point out that the degree of asymmetry shown by the PED depends on the value of the isosurface used for the representations of PED. To our knowledge, the dependency of the degree of asymmetry found in empty-state STM images on the tunnelling current has not been studied. However, such a correlation is expected from our calculations. The images of the electron densities near E_f obtained from tight-binding calculations of the extended Hückel type resemble the shapes of the frontier orbitals calculated with molecular models.[39] It is obvious that the phase vector of the wave function cannot generally be depicted, but the spatial extension and shapes of the frontier crystal orbitals (bands) in direct space are well represented by the PED. Therefore, using PED diagrams, we believe that the frontier orbital approach can be extended, with certain restrictions, to different fields of surface chemistry and to three-dimensional solids.

Whereas total and partial electron density are helpful in detecting the position of atoms (LEED and STM), they do not allow us to draw direct conclusions concerning the chemical bond. The electron-localization function, in principle, also an observable quantity,[12] visualizes surface regions with bonding and nonbonding properties in an unique manner. We showed that the orientation of the dangling bonds of the three-coordinate surface atoms of the topmost surface layer can be visualized. In the case of the symmetric surface dimer we see that electrons are localized between the surface atoms, with the degree of localization depending on the extent of band occupancy; further filling of the band finally results in the formation of one big localization "bubble" at each surface atom, corresponding to a lone pair and the bonding electron pair (smaller area). In the case of the buckled dimer, an electron count consistent with silicon leads to two distinguishable localized regions, reflecting the bonding electron pair and the lone pair at the outer silicon atom. Formal reduction of the system by one electron per surface atom leads to a localization of electrons at the inner silicon atom. Additionally, we find from PED and ELF representations that there is an empty hybrid localized at the silicon atoms of the second layer pointing toward the vacuum.

Various electron counts in a rigid band model are considered here, so as to gain an understanding of Lewis acid/base interactions at the surface. The methods allow a direct pictorial analysis of the interaction of a Lewis acid or base with atoms of the topmost layers. From Figure 6f it can be seen that a virtual partial electron density arising from the LUCO is found at Si(3). This means that a Lewis base might also find a reaction partner in the subsurface silicon atoms. This is interesting with regard to the mechanism of NH_3 dissociation on Si(100). From STM experiments carried out on a Si(100) surface exposed to NH_3, it was concluded that N atoms mostly occupy subsurface positions.[40]

Finally a π-type interaction along the bond connecting Si(1), Si(2) and Si(3) has been established and explained in terms of hyperconjugated orbitals of all three silicon atoms. However, it could not be confirmed that the bond between the silicon atoms of the surface dimer had typical double-bond characteristics. For all types of coordination found in the surface atoms of the two topmost layers of the buckled model, analagous examples in molecular or solid-state compounds can be found.

Applying three-dimensional representations of quantum-mechanical calculations is not just an aesthetic exercise, but helps in further understanding of specific physical properties (STM) and supports the chemist's view of localized chemical properties. We believe that the partial electron densities below and above the Fermi level will also help us develop a deeper understanding of the chemical bonding in solids. According to this concept, solid-state compounds could be regarded as penetrating substructures, held together, for example, by Lewis base/acid type interactions. This merges with the description of chemical twinning and the idea of intergrowth structures.[41]

Computational Details

The tight-binding calculations were carried out with the extended Hückel implementation of tight-binding theory (program EHMACC) [31] using the atomic parameters for silicon (H_{ii} (eV), ζ): −17.3, 1.383 for 3s; −9.2, 1.383 for 3p. In order to obtain comparable results for all calculations (unreconstructed and reconstructed Si(100) surfaces), a rectangular unit cell composed of a 16-layer slab and a set of 162 k points distributed over half of the first Brillouin zone were used. The real-space resolution of TED, PED and ELF required an extended k-point set, which was also used for the calculation of DOS, LDOS and COOP. The large number of k points was necessary for a reliable calculation of the PED images. For the two Si(100)-(2×1) surface models, the reconstruction was carried out on both sides of the 16-layer slab. All Si–Si distances were fixed at 2.35 Å.

To calculate the ELF [11] the same procedure as described in [12,13] was incorporated in the EHMACC program. ELF(x,y,z) decribes the pair probability of finding two electrons with the same spin within a given volume element of density $\rho(x,y,z)$ (c.f. the pair probability in the Hartree-Fock treatment [11,12] or the excess local kinetic energy due to Pauli repulsion [13]). Herafter ELF could be considered as a measure of the Pauli repulsion. All three-dimensional colour graphical representations, two-dimensional images and contour plots were generated with the programs COLTURE [42], GRAPA [43], and DENSPLOT [44], respectively.

Acknowledgement: We thank Prof. H. Neddermeyer for permission to reproduce the STM images shown in Figure 2 and Prof. A. Savin for valuable discussions concerning the ELF function. The support of the ETH Zürich and the Swiss National Science Foundation is gratefully acknowledged.

Received: April 1, 1995 [F112]

[1] For a review see: G. A. Somorjai, M. A. Van Hove, *Structure and Bonding, Vol. 38*, Springer, Berlin, Heidelberg, New York, **1979**. K. Christmann, *Surf. Sci. Rep.* **1988**, *9*, 1.

[2] a) E. L. Mutterties, T. N. Rhodin, E. Band, C. F. Brucker, W. R. Pretzer, *Chem. Rev.* **1979**, *79*, 91. E. L. Mutterties, R. M. Wexler, *Surv. Prog. Chem.* **1983**, *10*, 61. b) M. R. Albert, J. T. Yates Jr., *The Surface Scientist's Guide to Organometallic Chemistry*, American Chemical Society, Washington DC, **1987**. c) R. Hoffmann, *Solids and Surfaces*, VCH, New York, **1988**. d) J. K. Burdett, T. F. Fässler, *ibid.* **1992**, *31*, 129.

[3] G. N. Lewis, *J. Am. Chem. Soc.* **1916**, *38*, 762. G. N. Lewis, *Valence and the Structure of Atoms and Molecules*, Chemical Catalog, New York, **1923**.

[4] L. Pauling, *J. Am. Chem. Soc.* **1931**, *53*, 1367. J. C. Slater, *Phys. Rev.* **1931**, *37*, 481.

[5] R. Gillespie, R. S. Nyholm, *Quat. Rev. Chem. Soc.* **1957**, *11*, 339. R. J. Gillespie, *Chem. Educ.* **1963**, *40*, 295. R. Gillespie, *Angew. Chem.* **1976**, *79*, 885; *Angew. Chem. Int. Ed. Engl.* **1967**, *6*, 819. R. Gillespie, *Molecular Geometry*, Van Nostrand-Reingold, London, **1972**.

[6] K. Wade, *Adv. Inorg. Chem. Radiochem.* **1976**, *18*, 1.

[7] a) H. Weinstein, R. Pauncz, *Adv. At. Mol. Phys.* **1971**, *7*, 97. A. Reed, L. Curtiss, F. Weinhold, *Chem. Rev.* **1988**, *88*, 899. b) R. B. Woodward, R. Hoffmann, *The Conservation of Orbital Symmetry*, Academic Press, New York, **1969**. K. Fukui, *Theory of Orientation and Stereo Selection*, Springer, Berlin, **1975**.

[8] For detail see: N. W. Ashcroft, A. D. Mermin, *Solid State Physics*, Sounders College Publishing International Edition, Philadelphia, **1976**. W. Harrison, *Electronic Structure and the Properties of Solids*, Dover Publications, New York, **1980**.

[9] T. Hughbanks, R. Hoffmann, *J. Am. Chem. Soc.* **1983**, *105*, 3528.

[10] Recently a method of constructing localized orbitals from band orbitals (Wannier functions) using a probe orbital to choose the phase factor was applied to extended systems. See: K. A. Yee, T. Hughbanks, *Inorg. Chem.* **1991**, *30*, 2321. K. A. Yee, T. Hughbanks, *ibid.* **1992**, *31*, 1620. Y. Tian, T. Hughbanks, *ibid.* **1993**, *32*, 400.

0947-6539/95/0109-0632 $ 10.00+.25/0

[11] A. D. Becke, E. Edgecombe, *J. Chem. Phys.* **1990**, *92(9)*, 5397.

[12] A. Savin, A. D. Becke, J. Flad, R. Nesper, H. G. von Schnering, *Angew. Chem.* **1991**, *103*, 421; *Angew. Chem. Int. Ed. Engl.* **1991**, *30*, 409. A. Savin, H.-J. Flad, J. Flad, H. Preuss, H. G. von Schnering, *ibid.* **1992**, *104*, 185 and **1992**, *31*, 185. A. Burkhardt, U. Wedig, H. G. von Schnering, *Z. Anorg. Allg. Chem.* **1993**, *619*, 437. D. Seebach, H. M. Bürger, D. A. Plattner, R. Nesper, T. F. Fässler, *Helv. Chim. Acta* **1993**, *76*, 2581.

[13] a) A. Savin, O. Jepsen, J. Flad, O. Anderson, H. Preuss, H. G. von Schnering, *Angew. Chem.* **1992**, *104*, 186; *Angew. Chem. Int. Ed. Engl.* **1992**, *31*, 186. U. Häussermann, S. Wengert, P Hofmann, A. Savin, O. Jepsen, R. Nesper, *ibid.* **1994**, *106*, 2147 and **1994**, *33*, 2069. b) B. Silvi, A. Savin, *Nature* **1994**, *371*, 683. (c) U. Häussermann, S. Wengert, R. Nesper, *Angew. Chem.* **1994**, *106*, 2150; *Angew. Chem. Int. Ed. Engl.* **1994**, *33*, 2073.

[14] R. E. Schlier, H. E. Farnsworth, *Semiconducting Surface Physics*, University of Pennsylvania, Philadelphia, **1957**. W. Mönch, *Surf. Sci.* **1979**, *86*, 672. See also: Proceedings of the Fourth International Conference on Scanning Tunnelling Microscopy/Spectroscopy, *J. Vac. Sci. Technol. A* **1990**, *8(1)*, 153.

[15] a) R. E. Schlier, H. E. Farnsworth, *J. Chem. Phys.* **1959**, *30*, 917. b) J. Levin, *Surf. Sci.* **1973**, *90*, 90.

[16] F. Jona, J. D. Shih, D. W. Jepsen, P. M. Marcus, *J. Phys.* **1979**, *12*, L455. W. S. Yang, F. Jona, P. M. Marcus, *Solid State Commun.* **1982**, *43*, 847 and *Phys. Rev.* **1983**, *B28*, 2049.

[17] M. J. Cardillo, G. E. Becker, *Phys. Rev. Lett.* **1978**, *40*, 1148 and *Phys. Rev.* **1980**, *B21*, 1497. R. M. Tromp, R. G. Smeek, F. W. Saris, *Phys. Rev. Lett.* **1981**, *46*, 939.

[18] M. Aono, Y. Hou, C. Oshima, Y. Ishizawa, *Phys. Rev. Lett* **1982**, *49*, 567. I. Stensgaard, L. C. Feldmann, P. J. Silverman, *Surf. Sci.* **1981**, *102*, 1. R. M. Tromp, R. G. Smeek, F. W. Saris, D. J. Chadi, *ibid.* **1983**, *133*, 137.

[19] a) F. J. Himpsel, D. E. Eastman, *J. Vac. Sci. Technol.* **1979**, *16*, 1297. F. J. Himpsel, T. Fauster, *ibid.* **1984**, *A2*, 815. P. Martensson, A. Cricenti, G. V. Hansson, *Phys. Rev.* **1986**, *B33*, 8855. b) H. A. van Hoof, M. J. van der Wiel, *Appl. Surf. Sci.* **1980**, *6*, 444. G. J. R. Jones, B. W. Holland, *Solid State Commun.* **1983**, *46*, 651. S. J. White, D. C. Frost, K. A. R. Mitchell, *ibid.* **1982**, *42*, 763. W. Mönch, P. Koke, S. Krueger, *J. Vac. Sci. Technol.* **1981**, *19*, 313. B. W. Holland, C. B. Duke, A. Paton, *Surf. Sci.* **1984**, *140*, L269. G. Jayaram, P. Xu, L. D. Marks, *Phys. Rev. Lett.* **1993**, *21*, 3489.

[20] a) R. Wolkow, *Phys. Rev. Lett.* **1992**, *68*, 2636. b) R. J. Hamers, R. M. Tromp, J. E. Demuth, *Phys. Rev.* **1986**, *B34*, 5343 and references therein. R. M. Tromp, R. J. Hamers J. E. Demuth, *Phys. Rev. Lett.* **1985**, *55*, 1303. c) R. J. Hamers U. K. Köhler, *J. Vac. Sci. Technol.* **1989**, *A7*, 2854.

[21] a) P. Avouris, *J. Phys. Chem.* **1990**, *94*, 2246. G. P. Kochanski, J. E. Griffith, *Surf. Sci.* **1991**, *249*, L293. b) R. Wiesendanger, D. Bürgel, G. Tarrach, H.-J. Güntherodt, I. V. Shevts, J. M. D. Coy, *ibid.* **1992**, *274*, 93.

[22] a) H. Neddermeyer, *Chem. Unserer Zeit* **1992**, *26(1)*, 18. b) R. Kliese, B. Röttger, D. Badt, H. Neddermeyer, *Ultramicroscopy* **1992**, *42*, 824. c) M. J. Bronikowski, Y. Wang, M. T. McEllistrem, D. Chen, R. Hamers, *Surf. Sci.* **1993**, *298*, 50.

[23] a) E. Artacho, F. Yndurain, *Phys. Rev. Lett.* **1989**, 62, 2491. b) I. P. Batra, S. Ciraci, *ibid.* **1976**, *36*, 170. I. P. Batra, S. Ciraci, I. B. Ortenburger, *Solid State Commun.* **1976**, *18*, 563. W. S. Verwoerd, *Surf. Sci.* **1983**, *129*, 419. A. Redondo W. A. Goddard, *J. Vac. Sci. Technol.* **1982**, *21*, 344. I. P. Batra, *Phys. Rev.* **1990**, *B41*, 5048. M. C. Payne, N. Roberts, R. J. Needs, M. Needels, J. D. Joannopoulos, *Surf. Sci.* **1989**, *211/212*, 1. R. Caballol, R. Gallifa, J. M. Riera, R. Carbo, *Int. J. Quantum. Chem.* **1974**, 373. K. Pandey, in *Proceedings of the 17th International Conference on the Physics of Semiconductors* (Eds.: D. J. Cadi, W. A. Harrison), Springer, New York, **1985**, p. 55. Z. Jing, J. Whitten, *Surf. Sci.* **1992**, *274*. 106.

[24] a) D. J. Cadi, *Phys. Rev. Lett.* **1979**, *43*, 43. b) A. Mazur J. Pollmann, *Phys. Rev.* **1982**, *B26*, 7086. c) C. W. S. Verwoerd, *Surf. Sci.* **1980**, *99*, 581. *ibid.* **1981**, *103*, 404. P. Krüger, J. Pollmann, *Pys. Rev.* **1988**, *B38*, 10578. J. Ihm, M. l. Cohen, D. J. Chadi, *ibid.* **1980**, *B21*, 4592. G. P. Kerker, S. G. Louie, M. L. Cohen, *ibid.* **1978**, *B17*, 706. d) M. T. Yin, M. L. Cohen, *ibid.* **1981**, *B24*, 2303.

[25] F. Bechstedt, D. Reichardt, *Surf. Sci.* **1988**, *202*, 83. D. J. Cadi, *J. Vak. Sci. Technol.* **1979**, *16*, 1290. J. Ihm, D. H. Lee, J. D. Joannopoulos, A. N. Berker, *ibid.* **1983**, *B1*, 705. J. Ihm, D. H. Lee, J. D. Joannopoulos, J. J. Xiong, *Phys. Rev. Lett.* **1983**, *51*, 1872. P. Badziag, W. Voerwoerd, M. Van Hove, *Phys. Rev.* **1991**, *B43*, 2058.

[26] J. Dabrowski, M. Scheffler, *Appl. Surf. Sci.* **1992**, *56–58*, 15.

[27] a) J. A. Appelbaum, D. R. Hamann, *Surf. Sci.* **1978**, *74*, 21. J. A. Appelbaum, G. A. Baraff, D. R. Haman, **1975**, *35*, 729 *ibid.* **1976**, *B14*, 729. b) J. Ihm, M. L. Cohen, D. J. Chadi, *Phys. Rev.* **1980**, *B21*, 4592.

[28] J. Tersoff, D. R. Hamann, *Phys. Rev. Lett.* **1983**, *50*, 1998. *ibid.* **1985**, *B31*, 805. J. Tersoff, *J. Phys. Rev. Lett.* **1986**, *57*, 440.

[29] E. Tekman, S. Cirai, *Phys. Rev.* **1989**, *B40*, 10286.

[30] a) M. Tromp, R. J. Hamers, J. E. Demuth, *Science* **1986**, *234*, 304. b) S. N. Magonov, M.-H. Whangbo, *Adv. Mater.* **1994**, *6*, 355 and references therein.

[31] Programm EHMACC based on: R. Hoffmann, W. N. Lipscomb, *J. Chem. Phys.* **1962**, *36*, 2179; *ibid.* **1962**, *37*, 2872; and M.-H. Whangbo, R. Hoffmann, R. B. Woodward, *Proc. R. Soc. London* **1979**, *A366*, 23. Modification of the program for the calculation of TED, PED and ELF by U. Häussermann, R. Nesper, ETH Zürich.

[32] J. K. Burdett, S. Lee, *J. Am. Chem. Soc.* **1985**, *107*, 3063. J. K. Burdett, *Structure and Bondinding* **1987**, *65*, 29.

[33] Dimer tilt angles of 0–15° are discussed in ref. [20,24d,26].

[34] We want to point out here that the computation was done with a triclinic k point set within the first Brillouin zone, and not only with k points of high symmetry.

[35] This result reflects nicely the VSEPR rule that a nonbonding electron pair occupies more space than a bonding electron pair [5].

[36] J. Evers, *Solid State Chem.* **1979**, *28*, 369.

[37] W. Müller, H. Schäfer, A. Weiss, *Z. Naturforsch.* **1970**, *25B*, 1371.

[38] R. Probst, C. Leis, S. Gamper, E. Herdtweck, N. Auner, C. Zybill, *Angew. Chem.* **1991**, *103*, 1155; *Angew. Chem. Int. Ed. Engl.* **1991**, *30*, 1132.

[39] a) F. Iwawaki, H. Kato, M. Tomitori, O. Nishikawa, *Ultramicroscopy* **1992**, *42–44*, 895.

[40] R. J. Hamers, P. Avouris, F. Boszo, *Phys. Rev. Lett.* **1987**, *59*, 2071.

[41] B. G. Hyde, S. Andersson, *Inorganic Crystal Structures*, John Wiley, New York, **1989**.

[42] P. Hofmann, R. Nesper, Eidgenössische Techniche Hochschule Zürich, **1993**.

[43] J. Flad, F.-X. Fraschio, B. Miehlich, Program GRAPA, Institut für Theoretische Chemie der Universität Stuttgart 1989.

[44] S. Wengert, R. Nesper, Eidgenössische Techniche Hochschule Zürich, 1993.